Retraction Notice

Title of retracted article:	Heterojunction Photoelectrode of Polyaniline/ZnS Film/ZnO Nanorod on FTO Glass
Author(s):	Hyun Kim, B. Yang

* Corresponding author.   Email: h219@hanmail.net

Retraction initiative (multiple responses allowed; mark with **X**):
X All authors
☐ Some of the authors:
☐ Editor with hints from   Journal owner (publisher)
                                  Institution:
                                  Reader:
                                  Other:

Retraction type (multiple responses allowed):
☐ Unreliable findings
    Lab error   Inconsistent data   Analytical error   Biased interpretation
    Other:
☐ Irreproducible results
☐ Failure to disclose a major competing interest likely to influence interpretations or recommendations
☐ Unethical research

☐ Fraud
    Data fabrication   Fake publication   Other:
☐ Plagiarism   ☐ Self plagiarism   ☐ Overlap   ☐ Redundant publication *
☐ Copyright infringement   ☐ Other legal concern:

☐ Editorial reasons
    Handling error   Unreliable review(s)   Decision error   Other:

X Other:

Results of publication (only one response allowed):
X are still valid.
☐ were found to be overall invalid.

Author's conduct (only one response allowed):
☐ honest error
☐ academic misconduct
X none (not applicable in this case – e.g. in case of editorial reasons)

*   Also called duplicate or repetitive publication. Definition: "Publishing or attempting to publish substantially the same work more than once."

History
Expression of Concern:
☐ yes, date: yyyy-mm-dd
X no

Correction:
☐ yes, date: yyyy-mm-dd
X no

Comment:

This article has been retracted to straighten the academic record. In making this decision the Editorial Board follows COPE's Retraction Guidelines. Aim is to promote the circulation of scientific research by offering an ideal research publication platform with due consideration of internationally accepted standards on publication ethics. The Editorial Board would like to extend its sincere apologies for any inconvenience this retraction may have caused.

Heterojunction Photoelectrode of Polyaniline/ZnS Film/ZnO Nanorod on FTO Glass

Hyun Kim, B. Yang*

School of Advanced Materials Science and Engineering, Kumoh National Institute of Technology, Gumi, Republic of Korea
Email: *blyang@kumoh.ac.kr

Abstract

To enhance the absorption of visible light for wide-band-gap semiconductors, methods such as sensitizing with nanoparticles or quantum dots, and band gap engineering using dopants have been reported. However, these can cause lattice mismatch, inherent disorders, or imperfect charge balance, which serve as recombination sites and significantly reduce the photocatalytic efficiency. Herein, photoelectrodes of PANI/ZnS/ZnO on F:SnO₂ (FTO) were fabricated to analyze these issues and examine their interface microstructural and photocatalytic properties. ZnO nanorods (NRs) were grown on FTO glass by potentiostatic electrodeposition, and ZnS and PANI films were coated by liquid process. The PANI films were applied as a visible light sensitizer and photocorrosion prevention layer for ZnS/ZnO photoelectrodes. Subsequently, the prevention effect of photocurrent loss due to the photocorrosion of semiconductors was systematically investigated. The photocurrent of the PANI/ZnS/ZnO photoelectrode measured at 0.5V under white light illumination was five times higher than that of the ZnO NR photoelectrode. This was attributed to photocorrosion prevention and visible light absorption of PANI layers, due to proper energy band alignment of the hybrid heterojunction semiconductors.

Keywords

Polyaniline, Visible Light Sensitizer, Photocorrosion, Heterojunction, ZnS Shell/ZnO Core

1. Introduction

The solar energy received by the earth consists of ultraviolet (~5%) and visible light (~43%). Nanostructures are important not only for visible-light absorption in the solar spectrum, but also to obtain a high photocatalytic efficiency for semiconductor photoelectrodes. There has been extensive research on various nanostructured photoelectrodes such as nanowires, nanorods, and nanotubes

[1]-[6]. Many multilayered heterojunction nanostructures with great penetration depth have been also reported for the absorption of long wavelengths in the visible light spectrum, as well as the efficient charge separation and transfer of excited electrons and holes [7] [8] [9] [10].

One of the methods to enhance visible-light absorption is to adhere inorganic semiconductors with narrow-band-gap materials such as nanoparticles or quantum dots (QDs) on the surface of wide-band-gap semiconductors, as a sensitizer [11] [12] [13]. Another way is to manipulate the band gap sufficiently to obtain a visible light spectrum response of 1.7 - 2.9 eV by doping impurities such as carbon, nitrogen, or hydrogen [14] [15].

Regarding visible-light sensitizers, studies on chalcogenide compound QDs such as CdS (Eg = 2.4 eV), CdSe (1.7 eV), and CdSSe (1.9 eV) have been reported [16], as well as those on plasmonic Ag and Au nanoparticles [17], transition metal dichalcogenide sheets such as MoS_2 and WS_2 [18], and metal halide perovskites such as $CH_3NH_3PbI_3$ and $CsPbBr_3$ [20]. However, it is important to develop alternative sensitizer materials, owing to the significant disadvantages of the abovementioned materials, such as the harmful nature of Cd, high cost of noble metals, and unstable moisture process.

In band gap engineering through doping of single or several impurities, the recombination probability of excited electrons and holes is very high near doping sites, which include deteriorative crystal defects such as lattice mismatch at the interface between the sensitizer and wide-band-gap semiconductors, unstable inherent disorder [20], and charge imbalance among dopants. Hence, even though the absorption of visible light is improved by doping, these recombination sites can cause a significant loss of photocatalytic current during the separation and transfer of visible-light-excited electrons and holes.

Meanwhile, there are few reports on the photocorrosion of sensitizers such as QDs and nanoparticles attached on wide-band-gap semiconductors or those of semiconductors themselves. As alternatives, polymeric materials have recently been proposed as a prevention layer for photocorrosion. However, systematic studies on the photocatalytic performance using these films have not been reported thus far.

In this study, conductive organic polyaniline (PANI, $\Delta E_{\text{LUMO-HOMO}}$ = 2.4 eV) was applied for the core/shell composites of ZnS film/ZnO nanorods (NRs) on $F:SnO_2$ (FTO) substrates. Subsequently, the performance of PANI as a sensitizer as well as a prevention layer to improve the photocatalytic properties, was evaluated.

2. Methods

In this study, to fabricate the hybrid core/shell heterojunction photoelectrodes, after ZnO NRs were grown on FTO substrates by electrodeposition, ZnS films were formed on the surface of ZnO NRs by chemical dipping of ZnO NRs into Na_2S solution. Finally, the PANI films were coated by chemical dipping techniques. The detail processes are described below.

2.1. Preparation of ZnO NRs/FTO Glass Photoelectrode

ZnO NRs were grown on FTO (resistance = 8 $\Omega \cdot$m) glass by potentiostatic electrodeposition [21] [22]. The FTO glass was placed in an aqueous solution of 0.5 mM $ZnCl_2$ and 0.1 M KCl under oxygen bubbling in a three-electrode electrochemical cell, comprising a counter electrode of Pt mesh and reference electrode of Ag/AgCl/sat. KCl. Electrodeposition was carried out at −1.0 V for ~3 h at room temperature.

2.2. Particulate ZnS Film Coating on ZnO NRs

A particulate ZnS film was coated on the surface of the ZnO NRs by immersing the ZnO NR electrode in an aqueous 0.32 M $Na_2S \cdot 9H_2O$ solution for ~12 h. Sulfurization by anion-exchange reaction was carried out in a deionized water bath at 60°C. $Na_2S \cdot 9H_2O$ was used as an S^{2-} anion source to form ZnS on the surface of the ZnO NRs, according to the following reaction:

$$ZnO_{(s)} + S^{2-}_{(aq)} + H_2O_{(l)} \rightarrow ZnS_{(s)} + 2OH^-_{(aq)}$$

The electrode was then washed with deionized water and absolute ethanol several times and dried at 80°C for 1 h in an oven [23] [24].

2.3. PANI Sensitizer Coating on Particulate ZnS Film/ZnO NRs

The PANI sensitizer was coated by successive ionic layer adsorption and reaction using ammonium persulfate as an oxidizing agent. First, 0.4 M aniline was dissolved in 1 M sulfuric acid, which served as a cationic precursor in the first beaker. The second beaker contained an oxidant solution of 0.2 M ammonium persulfate in 1 M sulfuric acid, which served as an anionic precursor. The electrodes were then immersed into the aniline solution for 60 s for the surface polymerization of PANI on the particulate ZnS film/ZnO NR. Subsequently, the electrodes were immersed in the ammonium persulfate solution for 30 s [25] [26].

2.4. Microstructural Characterization

The microstructures of the photoelectrodes were characterized by field-emission scanning electron microscopy (FE-SEM; JSM-6500 F, JEOL), field-emission transmission electron microscopy (FE-TEM; 200 kV/JEM-2100F HR, JEOL), and X-ray diffraction (XRD, SWXD, Rigaku). Ultraviolet-visible (UV-vis) absorbance spectra of the electrodes were obtained using an ultraviolet-visible-near infrared (UV-VIS-NIR) spectrophotometer (UV 2600, Shimadzu). XPS was performed using a Thermo VG ESCALAB 250 instrument equipped with a microfocused, monochromatic A1 Kα X-ray source (1486.6 eV) and magnetic lens. The X-ray spot size was 500 μm (15 kV, 150 W). The spectra were acquired in the constant analyzer energy mode with a pass energy of 150 eV and 40 eV for overview scans and high-resolution scans, respectively.

2.5. Photoelectrochemical Characterization

The photocurrent densities of the photoelectrodes were measured using a potentiostat (AMT VERSASTAT 3, Princeton Applied Research) with a three-electrode cell comprising Pt mesh as the counter electrode and Ag/AgCl/sat. KCl as the reference electrode separated by a proton exchange membrane in aqueous 0.5 M Na_2SO_4 (pH = 7.15) electrolyte. Using a 1 kW xenon lamp (Newport) with the infrared wavelengths filtered out by water, 1 cm^2 of the working electrode was exposed. The light irradiance, measured using a thermopile detector, was 100 mW/cm^2.

3. Results and Discussion

3.1. Microstructural Characterization

In this study, photocatalytic properties of ZnS film/ZnO NR heterojunctions with PANI layers were investigated. For heterojunction composite fabrication, after the ZnO NRs were grown on FTO substrates by electroplating, ZnS layers were formed via sulfurization followed by PANI coating via cationic surface polymerization. The cross-sectional and surface FE-SEM images of ZnO NRs (**Figure 1**) show that the hexagonal ZnO NRs, with diameters of 300 - 500 nm and lengths of 0.5 - 1.5 μm, were grown vertically.
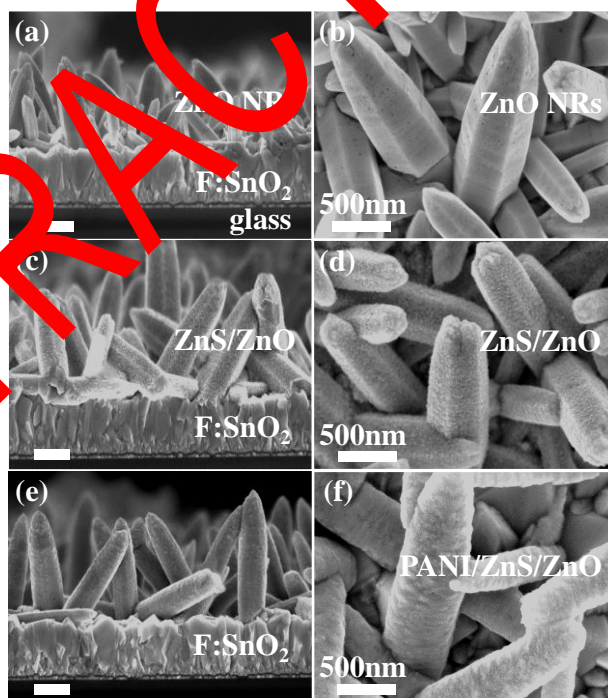

Figure 1. FE-SEM images of coated PANI on sulfurized ZnO NRs core. Cross sectional and surface views for ZnO NRs/FTO (a) & (b), particulate ZnS film/ZnO NRs/FTO (c) & (d), and PANI/particulate ZnS film/ZnO NRs/FTO (e) & (f), respectively.

The top surface of the prepared ZnO NRs was dominantly composed of slanted side faces of {10ī1} crystal planes rather than flat hexagonal {0001} crystal planes. Compared to the hexagonal {0001} planes, {10ī1} crystal planes have lower stacking density, and thus, higher surface energy. The hydrothermal growth

rate of ZnO NRs on FTO is determined primarily by the diffusion rate of Zn^{2+} ions during the process, and ion diffusion into side $\{10\bar{1}1\}$ planes is much more than that into top $\{0001\}$ surfaces, such that the hydrothermally grown ZnO NRs show wide $\{0001\}$ crystal planes on their top surfaces. On the other hand, electroplated ZnO NRs have narrow and sharp top surfaces composed of hexagonal $\{0001\}$ planes, because Zn^{2+} concentration is much higher in the top surfaces due to higher electroplating potential. However, many voids are observed on the surface of ZnO NRs (**Figure 1**), probably formed by O_2 gas bubbles in the electroplating bath, which disturbed the migration of Zn^{2+} ions on the surface.

Meanwhile, for fabrication of heterojunction composites with efficient charge separation, the ZnS films were coated on the surface of ZnO NRs via ion exchange sulfurization. When the ZnO NRs were dipped in the Na_2S solution, the O^{2-} ions on the ZnO surface and the S^{2-} ions in the Na_2S solution were exchanged to form ZnS particles on the surface of ZnO NRs. The cross-section and surface images of ZnS films/ZnO NRs fabricated by the processes are shown in **Figure 1(c)** and **Figure 1(d)**. As shown in **Figure 1(d)**, the ZnS films consist of stacked agglomerates of ~25 nm nanoparticles. The cross-section and top surface images of the conductive organic sensitizer, PANI, coated on the ZnS film/ZnO NRs are shown in **Figure 1(e)** and **Figure 1(f)**, respectively. As shown in **Figure 1(f)**, the smooth surface of a ZnO NR is surrounded by both ZnS film composed of stacked agglomerated nanoparticles and PANI film.

TEM images of PANI/ZnS film/ZnO NRs (**Figure 2(a)** and **Figure 2(b)**) show that a core electrodeposited ZnO NR is surrounded by both ~5-nm-thick PANI film and ~30-nm-thick particulate ZnS film. Thus, this core/shell structure should prevent direct contact of ZnO NRs with the electrolyte in the photocatalytic cells, thus preventing deterioration of photocatalytic current due to photocorrosion.

ZnS films on ZnO NRs can be typically formed by several methods like chemical absorption of ZnS nanoparticles and vapor-liquid-solid (VLS) methods.
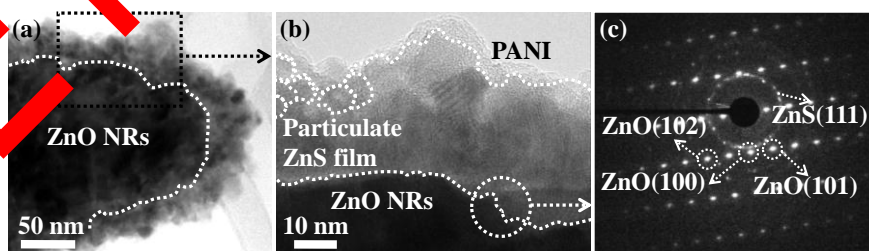

Figure 2. TEM (a) bright field and (b) lattice fringe images of the PANI/particulate ZnS film/ZnO NRs, and (c) selective area electron diffraction pattern of the interface between particulate ZnS film and ZnO NRs, respectively.

However, for direct adhesion of ZnS nanoparticles on the ZnO surface, micro-voids can occur in the sites between the ZnS nanoparticles. The lattice mismatch between the ZnS nanoparticles and ZnO NRs can also cause the interface defects. Thus, annealing processes are necessary for reduction of these crystalline defects.

In the VLS methods using Zn and S powder sources, non-uniform adsorption of

Zn and S vapors on the surfaces of ZnO NRs, which have different surface states depending on crystal orientations, results in anisotropic growth of ZnS. Thus, it is difficult to obtain dense ZnS films using this technique, but thick films can be obtained. However, in the surface sulfurization processes, uniform ZnS films can be feasibly formed, because ZnS nanoparticles are formed by ion exchange of O^{2-} ions on the ZnO surface and S^{2-} ions in the solution. Furthermore, the crystal orientations of ZnO NRs have negligible effect on the growth of ZnS because the ZnO surface is surrounded by water molecules in the solution.

The PANI film synthesized by polymerization was deposited relatively uniformly on the ZnS film. Selected area electron diffraction patterns for the interface between particulate ZnS film and ZnO NRs are shown in **Figure 2(c)**. Polycrystalline ring patterns and single-crystalline dot patterns were observed for the particulate ZnS film and the ZnO NR, respectively. Electron diffraction patterns from (100), (101), and (102) ZnO (zincite space group P63mc; JCPDS card no. 36-1451) for the [0$\bar{1}$0] zone axis were observed, confirming the hexagonal Wurtzite structure of ZnO NRs.

However, the electron diffraction patterns of the ZnS film corresponded to both the (111) sphalerite cubic phase (space group F43m; JCPDS card no. 05-0566) and the hexagonal (008) hexagonal phase (space group P63mc; JCPDS card no. 39-1363), which have interplanar distances of 3.123 Å and 3.120 Å, respectively. At this point, the structure of ZnS is not clear. However, other groups using similar ZnS synthesis processes reported cubic zinc blende (111) peaks at $2\theta = 28.62°$ in XRD patterns.

The XRD patterns for PANI/particulate ZnS film/ZnO NRs/FTO samples (**Figure 3**) indicate that the peaks ($2\theta = 31.8°, 34.5°, 36.3°, 47.6°, 56.5°,$ and $62.9°$) of ZnO NRs correspond to the (100), (002), (101), (102), (110), and (103) crystal planes, respectively, of the hexagonal crystal lattice of zincite (space group P63mc; JCPDS card no. 36-1451). The peak at $2\theta = 28.61°$ corresponds to the cubic ZnS (111) crystal plane. However, the XRD peaks of PANI layer were not observed. This resulted from the amorphous phase of the PANI layer after the synthesis and dip-coating, whereas other group has reported for the polycrystalline PANI synthesis. This discrepancy was attributed to different processes including sources for the PANI synthesis [27].

The PANI layer and compositional surface analysis of the ZnS film/ZnO NRs were characterized by using X-ray photoelectron spectroscopy (XPS), and the analysis results are shown in **Figure 4**. Zn $2p_{1/2}$ (1,045 eV), Zn $2p_{3/2}$ (1,020 eV) and O 1s (531 eV) peaks were observed for ZnO NRs, and S 2s (226 eV) and S 2p
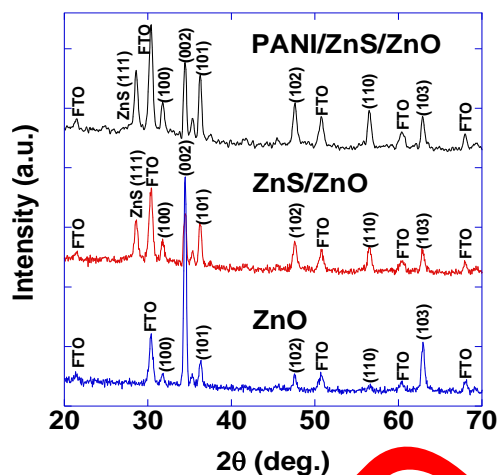
Figure 3. X-ray diffraction patterns of PANI/particulate ZnS film/ZnO NRs, ZnS/ZnO NRs, and ZnO NRs on FTO glass, respectively.
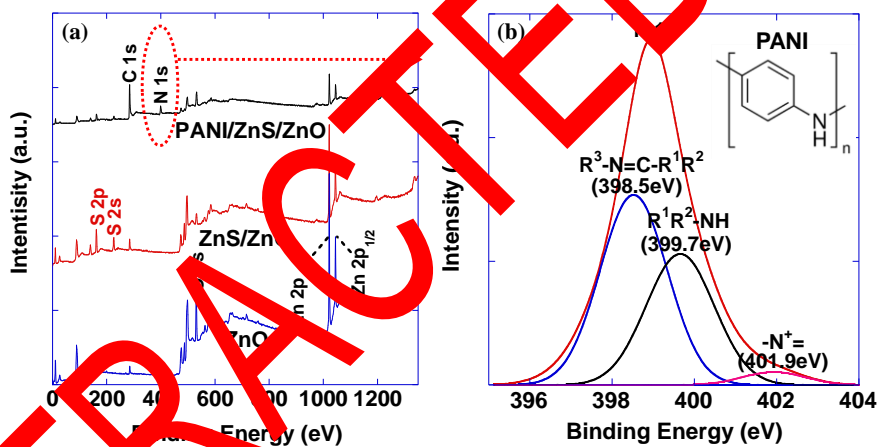

Figure 4. XPS spectra of (a) PANI/particulate ZnS film/ZnO NRs, particulate ZnS film/ZnO NRs and ZnO NRs, respectively, and (b) chemical element N 1s peak composed of imine as R^3–N = C-R^1R^2 (398.5eV), amine as R^1R^2-NH (399.7 eV) and protonated nitrogen as -N^+ = (401.9eV).

(162 eV) peaks were observed for ZnS films. On the other hand, N 1s (399 eV) and C 1s (285 eV) peaks were observed for PANI. The N 1s (399 eV) peak, consisting of imine R^3-N = C-R^1R^2 (398.5 eV), amine R^1R^2-NH (399.7 eV), and protonated nitrogen -N^+ = (401.9 eV) signals, originated from the N element of the aniline monomer, as shown in **Figure 4(b)** [28].

3.2. Photoelectrochemical Characterization

The UV-Vis absorption spectra of PANI/ZnS film/ZnO NRs, ZnS film/ZnO NRs, and ZnO NR electrodes were measured as shown in **Figure 5(a)**. All the spectra present a strong absorption in the UV region between 300 and 400 nm. The band gaps of each layers were estimated from the Tauc plots [29] as shown in **Figure 5(b)**. The values from the line intersections were measured as 3.12, 3.16, and 2.7 eV for ZnO NRs, ZnS film/ZnO NRs, and PANI/ZnS film/ZnO
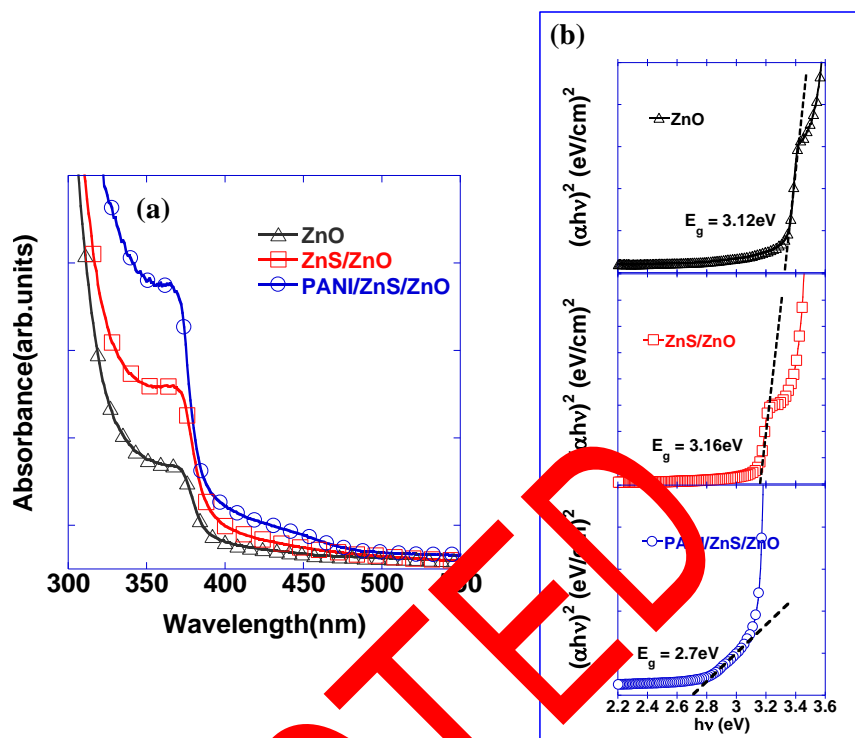
Figure 5. (a) UV-Vis absorption spectra and (b) tauc plot for band gap calculation of ZnO NRs, ZnS film/ZnO NRs, and PANI/ZnS film/ZnO NRs electrode, respectively.

NRs, respectively. The ZnO NRs coated with the ZnS film of the wide band gap showed slightly increased band gap, that is blue-shifting absorption. However, the wide and weak absorption in the visible region between 400 and 500 nm was observed for the PANI coated ZnS film/ZnO NRs sample. This resulted in the reduced band gap of 2.7 eV in the Tauc plot. Thus this is due to the narrow band gap of the PANI layer in the range from ~2.4 eV to ~2.8 eV [30].

Photocurrent densities of the samples were measured in a photoelectrochemical (PEC) cell under exposure of white light consisting of UV and visible light (see **Figure 6(a)** ZnO, **Figure 6(b)** ZnS/ZnO, and **Figure 6(c)** PANI/ZnS/ZnO, respectively). Photocurrent density corresponding to the pure photoresponse by using a chopping light source (on-off) was measured. The measured photocurrent density was the photoresponse difference between the on- and off-states of the light source.

Under white light illumination, the representative photocurrent densities of ZnO NRs, ZnS film/ZnO NRs, and PANI/ZnS film/ZnO NRs were 0.173 mA/cm^2, 0.461 mA/cm^2, and 0.865 mA/cm^2, respectively, at 0.5 V. The PANI/ZnS film/ZnO NR electrode showed about 5- and 1.8-times larger photocurrent density than the ZnO NRs and ZnS film/ZnO NRs, respectively. The ZnS film/ZnO NR electrode showed about 2.7-times larger photocurrent density than the ZnO NRs.

These measurement results confirm the light absorption spectral analysis results (**Figure 5**). The photocurrent densities of PANI/ZnS film/ZnO NRs were significantly improved due to superior visible light absorption properties of the
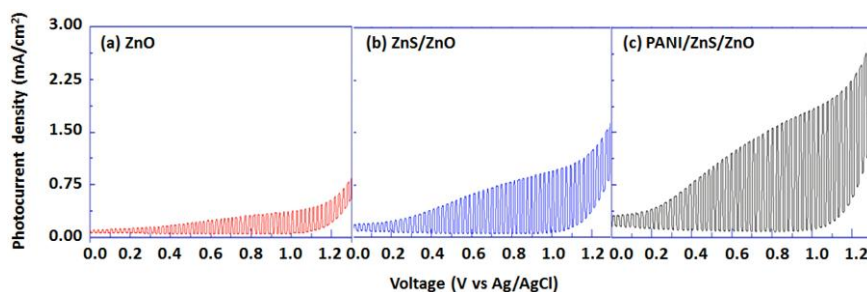
Figure 6. Photocurrent density of (a) ZnO NRs, (b) ZnS film/ZnO NRs, and (c) PANI/ZnS film/ZnO NRs electrodes under white light (UV and visible light) irradiation.

PANI layers. The PANI band gap was 2.7 eV as shown in **Figure 5(b)**. Furthermore, both PANI/ZnS film/ZnO NRs and ZnS film/ZnO heterojunction have good enough combination of potential levels (energy band alignment) to transfer and efficiently separate excited electrons and holes [31] [32] [33] [34].

In summary, PANI/ZnS film/ZnO NR photoelectrodes were fabricated and evaluated for their photocatalytic performance. Single-crystalline hexagonal ZnO NRs of lengths 0.5 - 1.5 µm were grown on FTO glass. Cubic ZnS films consisting of 5 - 10-nm nanoparticles were coated with thickness of ~30 nm on the ZnO NRs and organic PANI layers with thickness of ~5 nm were coated on the ZnS films. XRD and XPS analyses showed strong peaks for ZnS (111) and ZnO (002) crystal planes, and C/N elements and molecular bonding structure were observed for PANI.

4. Conclusion

In this study, PANI/ZnS/ZnO/FTO electrodes were studied on their interface and photocatalysis. Under white light illumination, the PANI/ZnS film/ZnO NR electrodes showed five times higher photocurrent density than ZnO NRs. This was due to the anti-photocorrosion and visible light absorption of PANI layer, and also provided proper energy band alignment of the hybrid heterojunction (PANI/ZnS film/ZnO NRs) to efficiently transfer and separate excited electrons and holes. It is expected that this hybrid heterojunction photoelectrode with proper band alignment using organic materials could be utilized for other applications such as photovoltaics, solar CO_2 fuel conversion, and solar pollutant decomposition.

Acknowledgements

Conflicts of Interest

The authors declare no conflicts of interest regarding the publication of this paper.

References

[1] Liu, B., Fang, Y., Li, Z. and Xu, S. (2015) Visible-Light Nanostructured Photocatalysts—A Review. *Journal of Nanoscience and Nanotechnology*, **15**, 889-920. https://doi.org/10.1166/jnn.2015.9784

[2] Valeeva, A.A., Kozlova, E.A., Vokhmintsev, A.S., Kamalov, R.V., Dorosheva, I.B., Saraev, A.A., Weinstein, I.A. and Rempel, A.A. (2018) Nonstoichiometric Titanium Dioxide Nanotubes with Enhanced Catalytical Activity under Visible Light. *Scientific Reports*, **8**, Article No. 9607. https://doi.org/10.1038/s41598-018-28045-1

[3] Li, C., Wang, H., Naghadeh, S.B., Zhang, J.Z. and Fang, P. (2018) Visible Light Driven Hydrogen Evolution by Photocatalytic Reforming of Lignin and Lactic Acid Using One-Dimensional NiS/CdS Nanostructures. *Applied Catalysis B*: *Environmental*, **227**, 229-239. https://doi.org/10.1016/j.apcatb.2018.01.038

[4] Kumar, S., Karthikeyan, S. and Lee, A.F. (2018) g-C₃N₄-Based Nanomaterials for Visible Light-Driven Photocatalysis. *Catalysts*, **8**, 74. https://doi.org/10.3390/catal8020074

[5] Tian, L., Rui, Y., Sun, K., Cui, W. and An, W. (2018) Surface Decoration of ZnWO₄ Nanorods with Cu₂O Nanoparticles to Build Heterostructure with Enhanced Photocatalysis. *Nanomaterials*, **8**, 33. https://doi.org/10.3390/nano8010033

[6] Ni, S., Zhou, T., Zhu, Y., Cao, Y. and Yang, P. (2018) Sn⁴⁺-Doped TiO₂ Nanorod Array Film with Enhanced Visible Light Photocatalytic Activity. *Bulletin of Materials Science*, **41**, 113. https://doi.org/10.1007/s12034-018-1629-8

[7] Velanganni, S., Pravinraj, S., Immanuel, P. and Thiruneelakandan, R. (2018) Nanostructure CdS/ZnO Heterojunction Configuration for Photocatalytic Degradation of Methylene Blue. *Physica B*, **534**, 56-62. https://doi.org/10.1016/j.physb.2018.01.027

[8] Sang, N.X., Tung, T.T., Huong, P.T.L., Tho, N.H. and Losic, D. (2018) Heterojunction of Graphene and Titanium Dioxide Nanotube Composites for Enhancing Photocatalytic Activity. *Journal of Physics D*: *Applied Physics*, **51**, Article ID: 265304. https://doi.org/10.1088/1361-6463/aac7ce

[9] Rampino, S., Pattini, F., Bronzoni, M., Mazzer, M., Sidoli, M., Spaggiari, G. and Gilioli, E. (2018) CuSbSe₂ Thin Film Solar Cells with ~4% Conversion Efficiency Grown by Low-Temperature Pulsed Electron Deposition. *Solar Energy Materials and Solar Cells*, **185**, 86-96. https://doi.org/10.1016/j.solmat.2018.05.024

[10] Cai, Y., Song, J., Liu, X., Lu, X., Li, X., Yu, J. and Ding, B. (2018) Soft BiOBr@TiO₂ Nanofibrous Membranes with Hierarchical Heterostructures as Efficient and Recyclable Visible-Light Photocatalysts. *Environmental Science-Nano*, **5**, 2631-2640. https://doi.org/10.1036/C8EN00866C

[11] Ye, C., Zhang, Y., Ding, A., Hu, Y. and Guo, H. (2018) Visible Light Sensitized Catalyzed Highly Selective Photo Oxidation from Thioethers into Sulfoxides Under Aerobic Condition. *Scientific Reports*, **8**, Article No. 2205. https://doi.org/10.1038/s41598-017-17765-5

[12] Athanas, A.B., Thangaraj, S. and Kalaiyar, S. (2018) Co-Sensitization of Ruthenium(II) Dye-Sensitized Solar Cells by Coumarin Based Dyes. *Chemical Physics Letters*, **699**, 32-39. https://doi.org/10.1016/j.cplett.2018.03.033

[13] Ouedraogo, S., Chouchene, B., Desmarets, C., Gries, T., Balan, L., Fournet, R., Medjahdi, G., Bayo, K. and Schneider, R. (2018) Copper Octacarboxy Phthalocyanine as Sensitizer of Graphitic Carbon Nitride for Efficient Dye Degradation under Visible Light Irradiation. *Applied Catalysis A*, **563**, 127-136. https://doi.org/10.1016/j.apcata.2018.06.036

[14] Rahaman, M.Z. and Hossain, A.K.M.A. (2018) Effect of Metal Doping on the Visible Light Absorption, Electronic Structure and Mechanical Properties of Non-Toxic Metal Halide CsGeCl₃. *RSC Advances*, **8**, 33010-33018. https://doi.org/10.1039/C8RA06374E

[15] Yang, Y., Yin, L.C., Gong, Y., Niu, P., Wang, J.Q., Gu, L., Chen, X., Liu, G., Wang, L. and Cheng, H.M. (2018) An Unusual Strong Visible-Light Absorption Band in Red Anatase TiO₂ Photocatalyst Induced by Atomic Hydrogen-Occupied Oxygen Vacancies. *Advanced Materials*, **30**, Article ID: 1704479. https://doi.org/10.1002/adma.201704479

[16] Kirkwood, N., Monchen, J.O.V., Crisp, R.W., Grimaldi, G., Bergstein, H.A.C., Fossé, I.D., Stam, W.V.D., Infante, I. and Houtepen, A.J. (2018) Finding and Fixing Traps in II-VI and III-V Colloidal Quantum Dots: The Importance of Z-Type Ligand Pas-

sivation. *Journal of the American Chemical Society*, **140**, 15712-15723.
https://doi.org/10.1021/jacs.8b07783

[17] Singh, A.N., Devnani, H., Jha, S. and Ingole, P.P. (2018) Fermi Level Equilibration of Ag and Au Plasmonic Metal Nanoparticles Supported on Graphene Oxide. *Physical Chemistry Chemical Physics*, **20**, 26719-26733.
https://doi.org/10.1039/C8CP05170D

[18] Nan, F., Li, P., Li, J., Cai, T., Ju, S. and Fang, L. (2018) Experimental and Theoretical Evidence of Enhanced Visible Light Photoelectrochemical and Photocatalytic Properties in MoS$_2$/TiO$_2$ Nanohole Arrays. *The Journal of Physical Chemistry C*, **122**, 15055-15062. https://doi.org/10.1021/acs.jpcc.8b01574

[19] Wu, Y., Wang, P., Zhu, X., Zhang, Q., Wang, Z., Liu, Y., Zou, G., Dai, Y., Whangbo, M.H. and Huang, B. (2018) Composite of CH$_3$NH$_3$PbI$_3$ with Reduced Graphene Oxide as a Highly Efficient and Stable Visible-Light Photocatalyst for Hydrogen Evolution in Aqueous HI Solution. *Advanced Materials*, **30**, Article ID: 1704342.
https://doi.org/10.1002/adma.201704342

[20] Potter, D.B., Powell, M.J., Parkin, I.P. and Carmalt, C.J. (2018) Aluminium/Gallium, Indium/Gallium, and Aluminium/Indium Co-Doped ZnO Thin Films Deposited via Aerosol Assisted CVD. *Journal of Materials Chemistry C*, **6**, 588-597.
https://doi.org/10.1039/C7TC04003B

[21] Frade, T., Siopa, D., Martins, A.F., Oliveira, J.F., Rodrigues, J., Sedrine, N.B., Correia, M.R., Monteiro, T., Zaera, R.T. and Gomes, A. (2018) Optoelectronic Characterization of ZnO Nanorod Arrays Obtained by Pulse Electrodeposition. *Journal of the Electrochemical Society*, **165**, D595-D603.
https://doi.org/10.1149/2.0121813jes

[22] Burgos, A., Schrebler, R., Cáceres, G., Dalchiele, E. and Gómez, H. (2018) Electrodeposition of ZnO Nanorods as Electron Transport Layer in a Mixed Halide Perovskite Solar Cell. *International Journal of Electrochemical Science*, **13**, 6577-6583.
https://doi.org/10.20964/2018.07.25

[23] Kao, C.H., Su, V.M., Li, C.H., Weng, W.C., Weng, C.Y., Cheng, C.C., Lin, Y.S., Lin, C.F. and Chen, H. (2018) Fabrication and Characterization of ZnS/ZnO Core Shell Nanostructures on Silver Wires. *AIP Advances*, **8**, Article ID: 065106.
https://doi.org/10.1063/1.5027015

[24] Ali, N.K., Rasoul, K.T.A. and Shanan, Z.J. (2013) New Method of Preparation ZnS Nano Size at Low pH. *International Journal of Electrochemical Science*, **8**, 3049-3056.

[25] Park, C.H., Jang, S.K. and Kim, F.S. (2018) Conductivity Enhancement of Surface-Polymerized Polyaniline Films via Control of Processing Conditions. *Applied Surface Science*, **429**, 121-127. https://doi.org/10.1016/j.apsusc.2017.09.031

[26] Karunagaran, R., Coghlan, C., Tran, D., Tung, T.T., Burgun, A., Doonan, C. and Losic, D. (2018) A Facile Synthesis Procedure for Sulfonated Aniline Oligomers with Distinct Microstructures. *Materials*, **11**, E1755.
https://doi.org/10.3390/ma11091755

[27] Talwar, V., Singh, O. and Singh, R.C. (2014) ZnO Assisted Polyaniline Nanofibers and Its Application as Gas Sensor. *Sensors and Actuators B*: *Chemical*, **191**, 276-282.
https://doi.org/10.1016/j.snb.2013.09.106

[28] Wei, X.L., Fahlman, M. and Epstein, A.J. (1999) XPS Study of Highly Sulfonated Polyaniline. *Macromolecules*, **32**, 3114-3117. https://doi.org/10.1021/ma981386p

[29] Awasthi, S., Gopinathan, P.S., Rajanikanth, A. and Bansal, C. (2018) Current-Voltage Characteristics of Electrochemically Synthesized Multi-Layer Graphene with Polyaniline. *Journal of Science*: *Advanced Materials and Devices*, **3**, 37-43.
https://doi.org/10.1016/j.jsamd.2018.01.003

[30] Trevizo, A.S., Madrid, P.A., Ruiz, P.P., Flores, W.A. and Yoshida, M.M. (2016) Optical Band Gap Estimation of ZnO Nanorods. *Materials Research*, **19**, 33-38.
https://doi.org/10.1590/1980-5373-mr-2015-0612

[31] Shuai, X.M. and Shen, W.Z. (2011) A Facile Chemical Conversion Synthesis of ZnO/ZnS Core/Shell Nanorods and Diverse Metal Sulfide Nanotubes. *The Journal of Physical Chemistry C*, **115**, 6415-6422. https://doi.org/10.1021/jp2005716

[32] Li, R., Wei, Z., Fang, X., Wang, Y., Li, Y., Wang, D., Tang, J., Fang, D., Chu, X., Yao, B., Chen, R. and Wang, X. (2018) Localized-State-Dependent Electroluminescence from ZnO/ZnS Core-Shell Nanowires-GaN Heterojunction. *ACS Applied Nano Materials*, **1**, 1641-1647. https://doi.org/10.1021/acsanm.8b00123

[33] Marana, N.L., Porta, F.A.L., Longo, E. and Sambrano, J.R. (2015) Theoretical Study on Band Alignment Mechanism for the ZnO@ZnS Interface of Core-Shell Structures. *Current Physical Chemistry*, **5**, 327-336. https://doi.org/10.2174/1877946805041600308170920

[34] Alam, M., Alandis, N.M., Ansari, A.A. and Shaik, M.R. (2013) Optical and Electrical Studies of Polyaniline/ZnO Nanocomposite. *Journal of Nanomaterials*, **2013**, Article ID: 157810. https://doi.org/10.1155/2013/157810